Phase-sensitive scanning tunneling potentiometry and the local transport field in mesoscopic systems

C. S. Chu and R. S. Sorbello
Department of Physics and Laboratory for Surface Studies, University of Wisconsin–Milwaukee, Milwaukee, Wisconsin 53201
(Received 16 February 1990)

A theoretical approach is presented to analyze the local transport field (LTF) and the voltage measured by the scanning tunneling microscope (STM) in a current-carrying mesoscopic system. The phase coherence between an electron wave reflected from a defect and the incident-electron wave leads to Friedel-like oscillations in both the LTF and STM voltage (V_{STM}). To study this phase-sensitive feature in scanning tunneling potentiometry, we calculate the spatial profile of LTF and V_{STM} for the case of grain boundaries in a thin film and for the case of an impurity near a surface. For the case of a thin film containing grain boundaries within the jellium model, we find that LTF and V_{STM} differ in their spatial variation, but their drops across a grain boundary are of the same order of magnitude. In general, the V_{STM} fluctuates on a larger length scale than the LTF. For the case of a scatterer on a metal surface, the short-range variations of both V_{STM} and the LTF near a surface scatterer are on the order of 1 μV when the current density is on the order of 10^7 A/cm^2 and the distance d between the STM tip and the metal surface is about 3 Å. Observation of the long-range variation in V_{STM} away from an impurity requires submicrovolt resolution and smaller values of d.

I. INTRODUCTION

The local transport field (LTF) is a local electric potential set up by the pileup of current carriers in the vicinity of defects when a transport current passes through a conductor.[1] It is the total LTF drop across a sample that contributes to the macroscopic voltage drop across the sample.[1,2] It follows that a complete description of electron transport should provide a correct LTF picture for both macroscopic and microscopic systems. In this respect, a direct experimental measurement of the LTF in the vicinity of an individual defect could provide a valuable check on electron-transport theory and would be of fundamental value.

Experimental techniques probing the LTF have been developed recently,[3–5] using the scanning tunneling microscope (STM) to simultaneously measure the surface topography and the spatial variations of the LTF across a grain boundary in a current-carrying conductor. In applying scanning tunneling potentiometry (STP), the STM tip is held at a fixed distance above the sample surface while the tip is scanned over the sample. The local potential in the sample is identified with the bias potential between the STP tip and the sample under the condition of zero tunneling current. A steplike drop of the experimentally determined STM voltage appears in the immediate vicinity of a grain boundary.[4,5] This is in qualitative agreement with the expected spatial variation of the LTF.[1,6] The question of whether the STP really measures the LTF was considered in our recent paper,[7] where we considered a grain boundary in a metal film and compared the voltage drop across the grain boundary measured by the STP (δV_{STM}) with the voltage drop in the LTF across the grain boundary (δV_{LTF}) for various film thicknesses. As we previously pointed out,[7] the LTF is essentially proportional to the local pileup of electron density associated with the electron-scattering states,[1,2,8,9] while the STM is more sensitive to those electron-wave functions that extend farther outside the surface.[7,10] Consequently, the electron states involved in the LTF do not contribute equally to the STM voltage, and δV_{STM} does not equal δV_{LTF} in general. However, we did find that δV_{STM} and δV_{LTF} are of the same order of magnitude, with δV_{STM} exhibiting larger quantum-size effects than δV_{LTF}.

In this paper, we compare the spatial profile of δV_{STM} and δV_{LTF}. Büttiker[11,12] pointed out that the phase-sensitive nature of voltage measurement can give rise to marked spatial oscillations in the STM voltage. This phase sensitivity is due to the fact that the reflected electron wave from the grain boundary or defect is still coherent with the incident electron wave in the neighborhood of the scatterer where the STM tip is positioned. Interference effects may then play an important role in the STM voltage. However, except for one-dimensional (1D) systems, there are two factors that diminish the phase-sensitivity effects as the STM tip moves away from localized scatterers. The first factor is the fanning out of the reflected electron wave, which results in decreasing interference as the distance from the scatterer is increased. The second factor is that, as more transverse states are involved, summing the contribution from these transverse states effectively introduces some phase averaging. The spatial variations of the STM potential that we obtain corroborate this viewpoint.

The outline of this paper is as follows. In Sec. II we introduce the general procedure to obtain the STM potential and the LTF.[7] The incident electron distribution is

taken to be of a general form and the geometry is a three-probe configuration[7,13] with the STM tip as an ideal probe, which probes only one point on the sample surface at a time. In Sec. III we apply the procedure to a specific system: a grain boundary in a thin-metal film. Three situations, which correspond to three different incident-electron distributions, are considered. The three situations are the reservoir case, the background relaxation-time case and the case of a random distribution of parallel semiclassical barriers. In the numerical examples, we compare the spatial variations of the LTF, the phase-sensitive STM potential and the phase-insensitive STM potential. The phase-insensitive STM potential is the potential when all interference effects are ignored, as in our previous paper.[7] In Sec. IV we apply the procedure to another system: a surface scatterer at a metal surface. Numerical examples are given for the incident-electron distribution determined by a background relaxation time τ. Finally, Sec. V presents a discussion.

II. GENERAL FRAMEWORK

In this section, we consider electron transport in mesoscopic systems, and we set up general expressions for the local transport field $\delta V_{\rm LTF}$ and the STM voltage $\delta V_{\rm STM}$ in terms of an incident electron distribution and the electron-scattering states.

As in our earlier work,[7] we describe the incident-electron distribution by effective channel-dependent chemical potentials $\mu_{L\alpha}$ and $\mu_{R\alpha}$, where α is the channel index. We define the channel index by the electron quantum numbers which correspond to motion perpendicular to the direction of the electron-transport current. We consider the system to have a rectangular cross section, with the electron transport occurring along direction $\hat{\mathbf{x}}$. It follows that $\alpha \equiv (k_y,k_z)$, where k_y and k_z are the transverse quantum numbers. The incident-electron states in a given channel α on the left-hand side (right-hand side) of the scattering region are taken to be occupied up to an energy $\mu_{L\alpha}$ ($\mu_{R\alpha}$) at zero temperature. The left-hand side (right-hand side) region refers to the negative-x (positive-x) region with respect to the scatterers. Since we shall assume the linear-response regime throughout, the quantities $\mu_{L\alpha}$ and $\mu_{R\alpha}$ differ only slightly from μ, the chemical potential for the equilibrium system in the absence of current flow. To simplify notation, we define the effective chemical potential of the incident electrons as

$$\mu_{\mathbf{k}} = \begin{cases} \mu_{L\alpha} & \text{for } k_x > 0 \\ \mu_{R\alpha} & \text{for } k_x < 0 \end{cases} , \tag{1}$$

where $\mathbf{k}=(k_x,k_y,k_z)$ and k_x refers to the wave vector of the electrons in the propagation direction. If $f^0(E_{\mathbf{k}})$ is the Fermi-Dirac distribution appropriate to chemical potential μ, then the incident-electron distribution is

$$f(E_{\mathbf{k}}) = f^0(E_{\mathbf{k}}+\mu-\mu_{\mathbf{k}}) = f^0(E_{\mathbf{k}})+\delta f_{\mathbf{k}} , \tag{2}$$

where, in the low-temperature regime considered here, it is an excellent approximation to take

$$\delta f_{\mathbf{k}} = \delta(E_{\mathbf{k}}-\mu)(\mu_{\mathbf{k}}-\mu) . \tag{3}$$

To derive an expression for $\delta V_{\rm LTF}$, we note that $\delta V_{\rm LTF}$ arises from the self-consistent screening of the local pile-up of electron number density, $\delta n_w(\mathbf{r})$, which is set up by the scattering of electrons by the defects. [$\delta n_w(\mathbf{r})$ is called an electron-wind contribution.[8]] Now, for a state $\psi^0_{\mathbf{k}}$ incident upon the defects, the scattering state is denoted by $\psi^{(+)}_{\mathbf{k}}$, and $\delta n_w(\mathbf{r})$ is given by

$$\begin{aligned} \delta n_w(\mathbf{r}) &= \sum_{\mathbf{k}} |\psi^{(+)}_{\mathbf{k}}(\mathbf{r})|^2 \delta f_{\mathbf{k}} \\ &= \sum_{\mathbf{k}} |\psi^{(+)}_{\mathbf{k}}(\mathbf{r})|^2 \delta(E_{\mathbf{k}}-\mu)(\mu_{\mathbf{k}}-\mu) . \end{aligned} \tag{4}$$

The electron pileup $\delta n_w(\mathbf{r})$ acts as an external charge distribution in an electron gas, and this gives rise to a self-consistent electron-screening response. In the linear-response regime considered here, the resulting self-consistent electrostatic potential energy of an electron, $\delta V_{\rm LTF}(\mathbf{r})$, is related to $\delta n_w(\mathbf{r})$ via a kernel $K(\mathbf{r},\mathbf{r}')$ in the usual way:[8]

$$\delta V_{\rm LTF}(\mathbf{r}) = \int K(\mathbf{r},\mathbf{r}')\delta n_w(\mathbf{r}')d^3r' . \tag{5}$$

The kernel $K(\mathbf{r},\mathbf{r}')$ is the response kernel for self-consistent screening in the absence of an electron current. The appearance of an equilibrium screening kernel is a consequence of our restriction to the linear regime of electron transport, where the chemical-potential difference $\mu_{L\alpha}-\mu_{R\alpha}$ is so small that the system response is linear in $\mu_{L\alpha}-\mu_{R\alpha}$. (Nonequilibrium corrections to $K(\mathbf{r},\mathbf{r}')$ are of order $\mu_{L\alpha}-\mu_{R\alpha}$, and would lead to contributions to $\delta V_{\rm LTF}$ which are second order in $\mu_{L\alpha}-\mu_{R\alpha}$ and are therefore negligible.)

Now $K(\mathbf{r},\mathbf{r}')$ is very difficult to determine because it describes the electron-screening response in the presence of the scatterer and any surfaces or interfaces of the system. Furthermore, $K(\mathbf{r},\mathbf{r}')$ should contain the effects of the scatterer, surfaces, or interfaces to all orders in their corresponding potentials. Rather than attempting to determine $K(\mathbf{r},\mathbf{r}')$ from a full self-consistent-field calculation for an inhomogeneous system, we resort to an approximation for $K(\mathbf{r},\mathbf{r}')$. In the simplest Thomas-Fermi approximation, Eq. (5) takes the form[1,8]

$$\delta V_{\rm LTF}(\mathbf{r}) = \frac{1}{e}(dn/dE)^{-1}\delta n_w(\mathbf{r}) , \tag{6}$$

where dn/dE is the electronic density of states at the Fermi level in the absence of scatterers and e is the charge of the electron. Equation (6) is a good approximation for 2D and 3D systems at distances beyond a few screening lengths from a scatterer and away from the immediate vicinity of a surface or interface. The approximation (6) works best when the screening length is small and the response is spatially averaged over a window on the order of a few screening lengths in size.

An improved Thomas-Fermi approximation would replace dn/dE in Eq. (6) by the local density of states at position $\mathbf{r}$ in the presence of the scatterers, surfaces, and interfaces.[13(a)] The resulting form of Eq. (6) is[13(b)]

$$\delta V_{\rm LTF}(\mathbf{r}) = \frac{\frac{1}{e}\sum_{\mathbf{k}} |\psi^{(+)}_{\mathbf{k}}(\mathbf{r})|^2 \delta(E_{\mathbf{k}}-\mu)(\mu_{\mathbf{k}}-\mu)}{\sum_{\mathbf{k}} |\psi^{(+)}_{\mathbf{k}}(\mathbf{r})|^2 \delta(E_{\mathbf{k}}-\mu)} , \tag{7}$$

where we have made use of expression (4) for $\delta n_w(\mathbf{r})$, and have introduced the explicit form for the local density of states in the denominator of Eq. (7).

Equations (6) and (7) give essentially the same $\delta V_{\rm LTF}$ for 2D and 3D systems in the region outside the immediate vicinity of scatterers, surfaces, or interfaces, especially when averaged over a few screening lengths. Unfortunately, even the result (7) arising from the improved Thomas-Fermi approximation is not very realistic in the immediate vicinity of scatterers, surfaces, and interfaces whose potentials vary over distances on the order of screening lengths, as is the typical case for metals. Consequently, expression (7) is likely to be only a marginal improvement over the simpler expression (6). In the numerical calculations to be reported later we used the simpler expression. More quantitative calculations of $\delta V_{\rm LTF}$ must await the availability of the full nonlocal kernel $K(\mathbf{r},\mathbf{r}')$ for scatterers in the vicinity of surfaces and interfaces.

Now we consider a STM tip located near the surface of the system. For a state $\psi_{\mathbf{k}}^0$ incident upon the defects, the charge current tunneling into state ν in the STM tip is

$$I_t(\mathbf{k};\nu)=\frac{2\pi e}{\hbar}|M(\mathbf{k};\nu)|^2\,\delta(E_{\mathbf{k}}-E_\nu)\ , \tag{8}$$

where $M(\mathbf{k};\nu)$ is the tunneling matrix element, $E_{\mathbf{k}}$ is the energy of the state $\psi_{\mathbf{k}}^0$, and E_ν is the energy of the state ν in the STM tip. The tunneling matrix element is of the form

$$|M(\mathbf{k};\nu)|^2=C_0|\psi_{\mathbf{k}}^{(+)}(\mathbf{r}_0)|^2\ , \tag{9}$$

where C_0 is a constant dependent only on the tip's properties and $\mathbf{r}_0$ is the position of the STM tip's center of curvature. Expression (9) was derived by Tersoff and Hamann[10] within the spherical-tip approximation in which the wave functions for electrons in the tip are approximated by their s-wave component. We emphasize that $\mathbf{r}_0$ is outside the system, and so $\psi_{\mathbf{k}}^{(+)}$ consists of exponential tails of various decay lengths.

Taking $\mu_{\rm STM}$ as the chemical potential in the STM tip, the total tunneling current $I_{\rm STM}$ into the STM tip is given by

$$I_{\rm STM}=\sum_\nu\sum_{\mathbf{k}} I_t(\mathbf{k};\nu)\delta(E_{\mathbf{k}}-\mu)(\mu_{\mathbf{k}}-\mu_{\rm STM})\ . \tag{10}$$

The $\mu_{\rm STM}$ is measured using the zero tunneling-current condition, i.e., $I_{\rm STM}=0$. The resulting expression for $\mu_{\rm STM}$ is

$$\mu_{\rm STM}(\mathbf{r}_0)=\frac{\sum_{\mathbf{k}}|\psi_{\mathbf{k}}^{(+)}(\mathbf{r}_0)|^2\,\delta(E_{\mathbf{k}}-\mu)\mu_{\mathbf{k}}}{\sum_{\mathbf{k}}|\psi_{\mathbf{k}}^{(+)}(\mathbf{r}_0)|^2\,\delta(E_{\mathbf{k}}-\mu)}\ . \tag{11}$$

The STM potential $V_{\rm STM}$ is related to $\mu_{\rm STM}$ through the expression

$$V_{\rm STM}(\mathbf{r}_0)=\mu_{\rm STM}(\mathbf{r}_0)/e\ , \tag{12}$$

which can be separated into two terms as follows:

$$V_{\rm STM}(\mathbf{r}_0)=\frac{\mu}{e}+\delta V_{\rm STM}(\mathbf{r}_0)\ . \tag{13}$$

The second term $\delta V_{\rm STM}$ in Eq. (13) is

$$\delta V_{\rm STM}(\mathbf{r}_0)=\frac{\frac{1}{e}\sum_{\mathbf{k}}|\psi_{\mathbf{k}}^{(+)}(\mathbf{r}_0)|^2\,\delta(E_{\mathbf{k}}-\mu)(\mu_{\mathbf{k}}-\mu)}{\sum_{\mathbf{k}}|\psi_{\mathbf{k}}^{(+)}(\mathbf{r}_0)|^2\,\delta(E_{\mathbf{k}}-\mu)}\ . \tag{14}$$

We emphasize that Eq. (14), unlike Eqs. (6) and (7), is not based upon any assumption concerning the electron-screening response.

It is tempting to conclude from the identical form of the right-hand sides of Eqs. (14) and (7) that the STM does indeed faithfully probe the local transport field. However, this conclusion is not correct because in Eq. (14) $\mathbf{r}_0$ refers to a point in the vacuum region outside the surface, while in Eq. (7) $\mathbf{r}$ refers to a point within the metallic system. What is at issue is whether $\delta V_{\rm STM}(\mathbf{r}_0)$ and $\delta V_{\rm LTF}(\mathbf{r})$ have the same spatial profile for $\mathbf{r}$ inside the system and $\mathbf{r}_0$ outside the system. Comparing $\delta V_{\rm LTF}$ and $\delta V_{\rm STM}$ in Eqs. (7) and (14), we see that the spatial dependence of the scattering state $\psi_{\mathbf{k}}^{(+)}$ plays an essential role in the overall spatial dependence. The exponential tails in $\psi_{\mathbf{k}}^{(+)}$ outside the system will favor the components of $\psi_{\mathbf{k}}^{(+)}$ that correspond to larger momentum perpendicular to the surface. Thus, in general, we do not expect $\delta V_{\rm LTF}$ and $\delta V_{\rm STM}$ to have the same spatial profile. Calculations of $\delta V_{\rm LTF}$ and $\delta V_{\rm STM}$, respectively, are presented in the following two sections.

III. GRAIN BOUNDARY IN A THIN-METAL FILM

In this section, we consider a grain boundary in a thin-metal film. The metallic thin film is taken to confine an electron gas by finite potential barriers. The confining potential $U_c(z)$ is given by

$$U_c(z)=\begin{cases}0, & -W/2<z<W/2\\ U_0, & |z|\geq W/2\ ,\end{cases} \tag{15}$$

where W is the thickness of the film. The unperturbed electron states $\psi_{n\mathbf{k}}^0$ in the film have the form

$$\psi_{n\mathbf{k}}^0(\mathbf{r})=\frac{e^{i\mathbf{k}\cdot\rho}}{\sqrt{A}}\phi_n(z)\ , \tag{16}$$

where A is the area of the film, $\mathbf{k}=(k_x,k_y)$, and $\rho=(x,y)$. Here n is the subband index and $\phi_n(z)$ satisfies the equation

$$\left[-\frac{\hbar^2}{2m^*}\frac{\partial^2}{\partial z^2}+U_c(z)\right]\phi_n(z)=E_n\phi_n(z)\ ,$$

where m^* is the effective mass. The energy of the state $\psi_{n\mathbf{k}}^0$ is $E_{n\mathbf{k}}=E_n+\hbar^2k^2/2m^*$. Since only the electrons near the Fermi level E_F are involved in the scattering, the magnitude of the wave vector $\mathbf{k}$ for an occupied subband (n) becomes k_{Fn}.

A grain boundary is taken to lie parallel to the y direction in the film and its potential U_B is modeled within the film as

$$U_B=\begin{cases}0, & x<0\\ fE_{FB}, & 0<x<\Delta\\ 0, & x>\Delta\ ,\end{cases} \tag{17}$$

where Δ is the width of the grain boundary, and the barrier height is expressed in units of E_{FB}, the bulk Fermi energy for a given electron density, with f being a dimensionless parameter. U_B is zero in the region outside the film. The modeling of the grain boundary as a potential barrier within the jellium model is a crude but useful approximation.[15] In the following analysis, we consider the case where the electron-transport current is perpendicular to the grain boundary and the transport electrons move along direction $\hat{x}$. To make connection with the notation introduced in the previous section, the channel index is defined as $\alpha\equiv(n,k_y)$, and the incident-electron distribution is described by $\mu_{L\alpha}$ and $\mu_{R\alpha}$ where the left-hand side region refers to the negative-x region and the right-hand side region refers to the positive-x region.

When a state $\psi^0_{n\mathbf{k}}$ of positive k_x is incident upon the grain boundary from the left-hand side, the scattering state is

$$\psi^{(+)}_{n\mathbf{k}}(\mathbf{r})=\frac{e^{ik_y y}}{\sqrt{A}}\times\begin{cases}e^{ik_x x}\phi_n(z)+\sum\limits_{n'} r_{nn'}(k_x)\phi_{n'}(z)e^{-ik_x(n')x}, & x<0\\ \sum\limits_{n'} t_{nn'}(k_x)\phi_{n'}(z)e^{ik_x(n')x}, & x>\Delta\end{cases} \tag{18}$$

and when a state $\psi^0_{n\mathbf{k}}$ of negative k_x is incident upon the grain boundary from the right-hand side, the scattering state is

$$\psi^{(+)}_{n\mathbf{k}}(\mathbf{r})=\frac{e^{ik_y y}}{\sqrt{A}}\times\begin{cases}\sum\limits_{n'} t'_{nn'}(|k_x|)\phi_{n'}(z)e^{-ik_x(n')x}, & x<0\\ e^{ik_x x}\phi_n(z)+\sum\limits_{n'} r'_{nn'}(|k_x|)\phi_{n'}(z)e^{ik_x(n')x}, & x>\Delta\ ,\end{cases} \tag{19}$$

where the summations are over all subbands and $r_{nn'},r'_{nn'}$ are the reflection coefficients while $t_{nn'},t'_{nn'}$ are the transmission coefficients. Here the effective wave vector along the $\hat{x}$ direction in subband (n') i s given by

$$k_x(n')=[(2m^*/\hbar^2)(E_n-E_{n'})+k_x^2]^{1/2}\ , \tag{20}$$

which can be imaginary if subband (n') is unoccupied. The conventional notation $(-1)^{1/2}=+i$ is adopted throughout. The summations in Eqs. (18) and (19) only include the subbands which have energies lower than the confining potential. This is a good approximation if we consider regions that are at a certain distance away from the grain boundary.[9] For the case of an ultrathin film with only a few propagating subbands, this distance is on the order of a few times λ_F, where λ_F is the bulk Fermi wavelength. For thick films, the distance is on the order of λ_F. We note that Equations (18) and (19) have contributions from propagatimg channels, i.e., the occupied subbands, as well as from the evanescent components, i.e., the unoccupied subbands.

We perform the summation over k_x and k_y in δn_w, given by Eq. (4), and find

$$\delta n_w(\mathbf{r})=\frac{m^*A}{\pi^2\hbar^2}\sum_n\int_0^{\pi/2}d\theta[|\psi^{(+)}_{n,\mathbf{k}_n^+}(\mathbf{r})|^2(\mu_{L\alpha}-\mu)+|\psi^{(+)}_{n,\mathbf{k}_n^-}(\mathbf{r})|^2(\mu_{R\alpha}-\mu)]\ , \tag{21}$$

where $\mathbf{k}_n^{\pm}\equiv k_{Fn}(\pm\cos\theta\,\hat{x}+\sin\theta\,\hat{y})$ and the summation is over all occupied subbands. For a grain boundary in a thin film, it is appropriate to consider the thickness-averaged local transport field. We note that the density of states within the film is

$$\frac{dn}{dE}\cong\frac{mN}{\pi\hbar^2W}\ , \tag{22}$$

where N is the total number of occupied subbands. The approximation (22) is valid when the extension of $\phi_n(z)$ into the vacuum is much smaller than W. The thickness-averaged local transport field is then given by

$$\overline{\delta V^L_{\mathrm{LTF}}(\rho)}=\frac{1}{eN\pi}\sum_n\int_0^{\pi/2}d\theta\left[\left[1+\sum_{n'}|r_{nn'}(k_{Fn}\cos\theta)|^2e^{2\,\mathrm{Im}[k_x(n')]x}+2\,\mathrm{Re}[r_{nn}(k_{Fn}\cos\theta)e^{-2ik_{Fn}\cos\theta x}]\right](\mu_{L\alpha}-\mu)\right.$$
$$\left.+\sum_{n'}|t'_{nn'}(k_{Fn}\cos\theta)|^2e^{2\,\mathrm{Im}[k_x(n')]x}(\mu_{R\alpha}-\mu)\right] \tag{23a}$$

and

$$\overline{\delta V^R_{\rm LTF}(\rho)}=\frac{1}{eN\pi}\sum_n\int_0^{\pi/2}d\theta\left[\sum_{n'}|t'_{nn'}(k_{Fn}\cos\theta)|^2e^{-2\,{\rm Im}[k_x(n')]x}(\mu_{L\alpha}-\mu)\right.$$
$$\left.+\left[1+\sum_{n'}|r'_{nn'}(k_{Fn}\cos\theta)|^2e^{-2\,{\rm Im}[k_x(n')]x}+2\,{\rm Re}[r'_{nn}(k_{Fn}\cos\theta)e^{2ik_{Fn}\cos\theta x}]\right](\mu_{R\alpha}-\mu)\right], \tag{23b}$$

where $\overline{\delta V^L_{\rm LTF}}$ and $\overline{\delta V^R_{\rm LTF}}$ are the thickness-averaged LTF for $x<0$ and $x>\Delta$, respectively, and $k_x(n')=[(2m^*/\hbar^2)(E_n-E_{n'})+k_{Fn}^2\cos^2\theta]^{1/2}$. Evanescent wave components occur in the LTF when $k_x(n')$ is imaginary. In obtaining Eqs. (23a) and (23b), we have substituted Eqs. (21), (22), (18), and (19) into Eq. (4) and then averaged the result over the width W spanned by the subband wave function $\phi_n(z)$.

Similarly, we perform the summation over k_x and k_y in the general expression (14) for $\delta V_{\rm STM}$ and find

$$\delta V_{\rm STM}(\mathbf{r}_0)=\frac{1}{e}\frac{\sum_n\int_0^{\pi/2}d\theta[|\psi^{(+)}_{n,\mathbf{k}_n^+}(\mathbf{r}_0)|^2(\mu_{L\alpha}-\mu)+|\psi^{(+)}_{n,\mathbf{k}_n^-}(\mathbf{r}_0)|^2(\mu_{R\alpha}-\mu)]}{\sum_n\int_0^{\pi/2}d\theta[|\psi^{(+)}_{n,\mathbf{k}_n^+}(\mathbf{r}_0)|^2+|\psi^{(+)}_{n,\mathbf{k}_n^-}(\mathbf{r}_0)|^2]}, \tag{24}$$

where the summation is over occupied subbands. The full expression of $\delta V_{\rm STM}$ in terms of all the reflection and transmission coefficients can be obtained by a direct substitution of Eqs. (18) and (19) into Eq. (24), and will not be given here explicitly.

The analysis so far is quite general for the case of a grain boundary in a metal film except that the grain boundary must preserve the translational invariance along the $\hat{y}$ direction within the film and that we must stay away from the immediate vicinity of the grain boundary, as mentioned after Eq. (20). In the following, we introduce the further approximation of neglecting interchannel scattering. This should be a good approximation for strong confining potentials, as is the case for metal films. (For $U_0=\infty$ it is exact.) The reflection coefficients are then given by[7]

$$r_{nn}(k_x)=r(k_x)=\frac{fk_{FB}^2\sinh(K\Delta)}{2iKk_x\cosh(K\Delta)+(k_x^2-K^2)\sinh(K\Delta)}, \tag{25}$$

and

$$r'_{nn}(k_x)=r'(k_x)=r(k_x)e^{-2ik_x\Delta}, \tag{26}$$

where $K=(fk_{FB}^2-k_x^2)^{1/2}$ and k_{FB} is the bulk Fermi wave vector. f is the barrier-strength parameter defined via Eq. (17). Here k_x is taken to be positive. In this approximation, the LTF Eqs. (23a) and (23b) reduce to

$$\overline{\delta V^L_{\rm LTF}(\rho)}=\frac{1}{eN\pi}\sum_n\int_0^{\pi/2}d\theta[\mu_{L\alpha}+\mu_{R\alpha}-2\mu+R(k_{Fn}\cos\theta)(\mu_{L\alpha}-\mu_{R\alpha})+2(\mu_{L\alpha}-\mu)G_n(\theta,x)], \tag{27a}$$

and

$$\overline{\delta V^R_{\rm LTF}(\rho)}=\frac{1}{eN\pi}\sum_n\int_0^{\pi/2}d\theta[\mu_{L\alpha}+\mu_{R\alpha}-2\mu-R(k_{Fn}\cos\theta)(\mu_{L\alpha}-\mu_{R\alpha})+2(\mu_{R\alpha}-\mu)G_n(\theta,\Delta-x)], \tag{27b}$$

where $R=|r|^2$ and $T=|t|^2=|t'|^2=1-R$, and

$$G_n(\theta,x)={\rm Re}[r(k_{Fn}\cos\theta)e^{-2ik_{Fn}\cos\theta x}].$$

Evaluating the STM voltage expression (24), we find that

$$\delta V^L_{\rm STM}(\mathbf{r}_0)=\frac{\frac{1}{e}\sum_n|\phi_n(z_0)|^2\int_0^{\pi/2}d\theta[\mu_{L\alpha}+\mu_{R\alpha}-2\mu+R(k_{Fn}\cos\theta)(\mu_{L\alpha}-\mu_{R\alpha})+2(\mu_{L\alpha}-\mu)G_n(\theta,x_0)]}{2\sum_n|\phi_n(z_0)|^2\int_0^{\pi/2}d\theta[1+G_n(\theta,x_0)]} \tag{28a}$$

and

$$\delta V^R_{\rm STM}(\mathbf{r}_0)=\frac{\frac{1}{e}\sum_n|\phi_n(z_0)|^2\int_0^{\pi/2}d\theta[\mu_{L\alpha}+\mu_{R\alpha}-2\mu-R(k_{Fn}\cos\theta)(\mu_{L\alpha}-\mu_{R\alpha})+2(\mu_{R\alpha}-\mu)G_n(\theta,\Delta-x_0)]}{2\sum_n|\phi_n(z_0)|^2\int_0^{\pi/2}d\theta[1+G_n(\theta,x_0-\Delta)]}. \tag{28b}$$

From Eqs. (27a) and (27b) and (28a) and (28b) it is apparent that $\delta V_{\rm STM}$ and $\delta V_{\rm LTF}$ are not equal. The $\delta V_{\rm STM}$ is more sensitive to the higher-occupied subbands because of the weighting factor $|\phi_n(z_0)|^2$ which is the exponential tail[16] of subband (n) electron density outside the surface region. In the case of one occupied subband, the spatial variation of $\delta V_{\rm LTF}$ and $\delta V_{\rm STM}$ are different because of the extra spatial dependent term in the denominator of $\delta V_{\rm STM}$; however, the spatial variation scale is the same, being determined by the effective k_x of the occupied subband. For the case of more than one occupied subband, the spatial variation of $\delta V_{\rm STM}$ is dominated by the spatial variation in subbands closest to the highest-occupied subband. This then implies that $\delta V_{\rm STM}$ has a longer variation scale than does $\delta V_{\rm LTF}$. This feature has been pointed out also by Büttiker.[12] That the $\delta V_{\rm STM}$ is able to pick up the interference between an incident-electron wave and the wave reflected from the grain boundary is shown by the existence of the interference term G_n in both the numerator and the denominator of $\delta V_{\rm STM}$. It is the interference that gives rise to the spatial dependence in $\delta V_{\rm STM}$, and to phase-sensitive scanning tunneling potentiometry. Dropping this interference term from the $\delta V_{\rm STM}$ expression leads to the phase-insensitive STP result, which is characterized by a constant $\delta V_{\rm STM}$ on each side of the grain boundary. Equations (28a) and (28b) also show that some phase averaging occurs as we sum the contributions from all possible k_y channels within the same subband. Hence, except for the one dimensional case, the deviation of the phase-sensitive result from the phase-insensitive result is expected to decrease as the STM tip moves away from the grain boundary.

The analysis thus far has not specified the form of $\mu_{L\alpha}$ and $\mu_{R\alpha}$. In the following we consider three different cases:[7] the reservoir case, the background scatterers case, and the case of a random distribution of parallel semiclassical barriers. For the reservoir case, we have

$$\mu_{L\alpha}=\mu+\Delta\mu \ , \tag{29a}$$

and

$$\mu_{R\alpha}=\mu \ . \tag{29b}$$

This corresponds to the situation in which the grain boundary is connected through perfect film conductors to two incoherent reservoirs, one on each side of the grain boundary. The chemical potentials of the two reservoirs are characterized by $\mu_{L\alpha}$ and $\mu_{R\alpha}$ as given in Eqs. (29a) and (29b). For the background-scatterer case, we have $\mu_{L\alpha}=\mu+\Delta\mu_\alpha$ and $\mu_{R\alpha}=\mu-\Delta\mu_\alpha$, where[7]

$$\Delta\mu_\alpha=eE_0 l\frac{k_{Fn}}{k_{FB}}\cos\theta \ , \tag{30}$$

and where E_0 is the x component of the electric field set up by the background τ and l is the bulk mean free path. This is the situation when the conducting film on either side of the grain boundary contains background scatterers which can be characterized by a collision time τ. For the case of random distribution of parallel semiclassical barriers, we have $\mu_{L\alpha}=\mu+\Delta\mu_\alpha$ and $\mu_{R\alpha}=\mu-\Delta\mu_\alpha$, where $\Delta\mu_\alpha$ is given by[7]

$$\Delta\mu_\alpha=\frac{e\delta V}{2R(k_{Fn}\cos\theta)} \ , \tag{31}$$

where δV is the total voltage drop across the sample divided by the number of barriers. In obtaining Eq. (31), coherent multiple scattering between barriers is neglected, as in Landauer's original treatment.[1,6] This should be a reasonable first approximation for weak-scattering grain boundaries in the absence of appreciable background scattering, though some incoherent background scattering should exist to remove the long-range, coherent inter-grain-boundary multiple scattering.

For numerical examples in the three cases, we take the film to be an aluminum film. The bulk Fermi wave vector k_{FB} equals 0.927 a.u. and $U_0=1.36E_{FB}$, which we obtain from the aluminum work function. For the grain boundary potential parameters in Eq. (17) we choose $f=0.2$ and $\Delta=4$ a.u. The distance d of the STM tip to the film surface is chosen to be 9.4 a.u. and the film thickness W is chosen to be 60 a.u. With this film thickness, the number of occupied subbands N is 18. The numerical examples have all assumed that the transport electrons move from left to right, along direction $\hat{x}$. Hence $\Delta\mu$ in Eq. (29a) is positive while E_0 and δV in Eqs. (30) and (31), respectively, are negative.

In Fig. 1 we present a plot of $\overline{\delta V_{\rm LTF}}$, $\delta V_{\rm STM}$, and the phase-insensitive $\delta V_{\rm STM}$ versus the STM tip distance from the grain boundary for the reservoir case. The vertical axis is in units of $\Delta\mu/|e|$ and the horizontal axis is in atomic units (Bohr radii). The grain boundary is shown in the figure also. The $\delta V_{\rm STM}$ plot is the curve that oscillates about the phase-insensitive $\delta V_{\rm STM}$ value which is indicated by the dashed line. On the left-hand side of the grain boundary, $\delta V_{\rm STM}$ has a longer variation scale than the $\overline{\delta V_{\rm LTF}}$. However, on the right-hand side of the grain boundary, the $\overline{\delta V_{\rm LTF}}$ becomes a constant indicated by a solid horizontal line. This is due to our assumption that all excess electrons come from the left-hand side, which gives no interference on the right-hand side of the grain boundary. We note that the drops across the grain boundary for $\overline{\delta V_{\rm LTF}}$ and $\delta V_{\rm STM}$ differ by a factor slightly larger than 2 and hence are of the same order of magnitude.

In Fig. 2 we present a plot of $\overline{\delta V_{\rm LTF}}$, $\delta V_{\rm STM}$, and the phase-insensitive $\delta V_{\rm STM}$ versus position from the grain boundary for the background-scatterer case. The vertical axis is in units of $|E_0 l|$. Again, the $\delta V_{\rm STM}$ curve oscillates about the phase-insensitive $\delta V_{\rm STM}$ value which is indicated by the dashed line. The $\delta V_{\rm STM}$ has a longer variation scale than the $\overline{\delta V_{\rm LTF}}$. All the three potentials are odd functions of the distance from the grain boundary, measured relative to the nearest edge of the grain boundary. We note that the drops across the grain boundary for $\overline{\delta V_{\rm LTF}}$ and $\delta V_{\rm STM}$ differ by a factor slightly larger than 1 and hence are of the same order of magnitude.

In Fig. 3 we present a plot of $\overline{\delta V_{\rm LTF}}$, $\delta V_{\rm STM}$, and the phase-insensitive $\delta V_{\rm STM}$ versus position from the grain boundary for the case of a random distribution of parallel

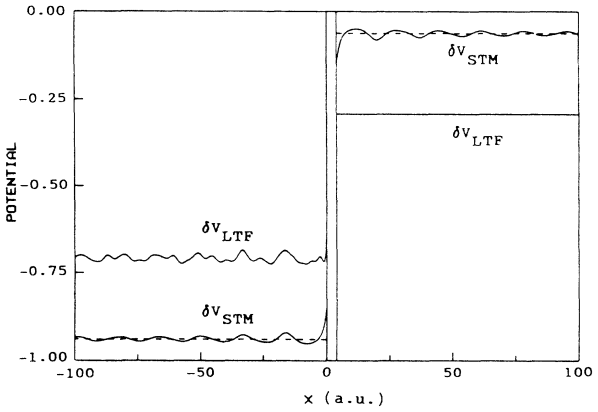

FIG. 1. $\overline{\delta V_{\mathrm{LTF}}}$, δV_{STM}, and the phase-insensitive δV_{STM} plotted against x for the reservoir case when a grain boundary is in an aluminum film of thickness 60 a.u. The vertical axis is in units of $-\Delta\mu/e$ and the horizontal axis is in atomic units. The region of the grain boundary is $0 \le x \le 4$ a.u. The STM tip height is 9.4 a.u., and the grain-boundary potential parameter $f=0.2$. The phase-insensitive δV_{STM} is indicated by the dashed line.

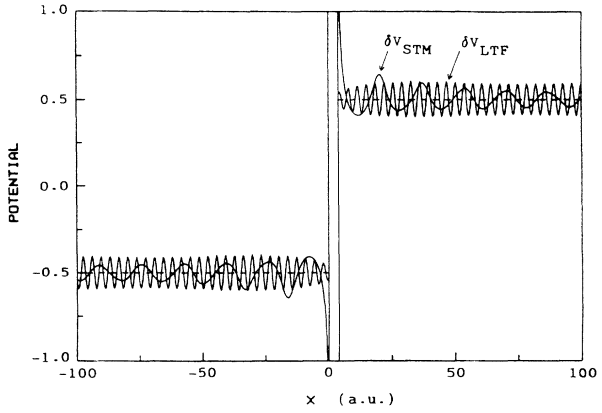

FIG. 3. $\overline{\delta V_{\mathrm{LTF}}}$, δV_{STM}, and the phase-insensitive δV_{STM} plotted against x for the case of random distribution of parallel semiclassical barriers. The vertical axis is in units of $|\delta V|$ and the horizontal axis is in atomic units. Other parameters are the same as in Fig. 1. The phase-insensitive δV_{STM} is indicated by the dashed line. Both the $\overline{\delta V_{\mathrm{LTF}}}$ and the δV_{STM} oscillate about the dashed line. The δV_{STM} curve has a longer wavelength.

semiclassical barriers. The vertical axis is in units of $|\delta V|$. In this case both δV_{STM} and $\overline{\delta V_{\mathrm{LTF}}}$ oscillate about the phase-insensitive δV_{STM} value indicated by the dashed line. The δV_{STM} still has a longer variation scale than the $\overline{\delta V_{\mathrm{LTF}}}$. All the three potentials are odd functions of the distance from the grain boundary. We note that the drops across the grain boundary for $\overline{\delta V_{\mathrm{LTF}}}$ and δV_{STM} differ by a factor close to 1.

Besides the above three examples, we examined other cases of different film thickness, including cases when there is only one occupied subband. All in all the numerical results are consistent with our aforementioned qualitative picture, that δV_{STM} and $\overline{\delta V_{\mathrm{LTF}}}$ do not have the same spatial profile, that δV_{STM} has a longer variation

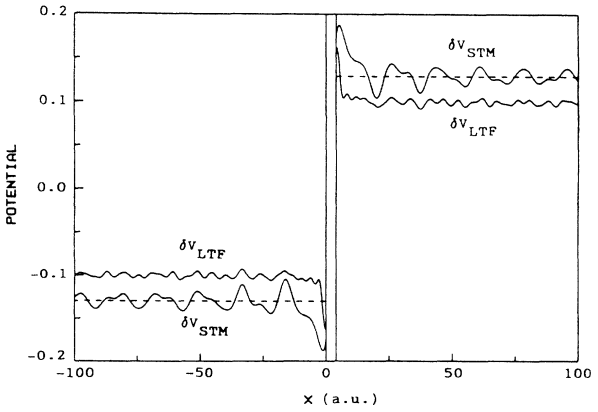

FIG. 2. $\overline{\delta V_{\mathrm{LTF}}}$, δV_{STM}, and the phase-insensitive δV_{STM} plotted against x for the background-scatterer case when a grain boundary is in an aluminum film. The vertical axis is in units of $|E_0 l|$ and the horizontal axis is in atomic units. Other parameters are the same as in Fig. 1. The phase-insensitive δV_{STM} is indicated by the dashed line.

scale than that of $\overline{\delta V_{\mathrm{LTF}}}$, except in the case of one occupied subband, and that the phase-sensitive spatial variations in δV_{STM} diminish gradually with increasing distance from the grain boundary, except in the case of one occupied subband. We remark that the spatial fluctuation in δV_{STM} away from the grain boundary should be experimentally observable.

To make connection with the experiments of Kirtley *et al.*,[4] we consider the random-barrier model and choose $W \approx 1200$ a.u. Using the current density appropriate to these experiments ($J \sim 10^7$ A/cm^2), we find that the drop in δV_{STM} across the grain boundary is on the order of 200 μV, which is in agreement with the measured value. Our calculated fluctuation amplitude of δV_{STM} away from the grain boundary is about 1% of the voltage drop across the grain boundary. This fluctuation amplitude, which is on the order of microvolt, is at least an order of magnitude smaller than observed by Kirtley *et al.*,[4] in addition, the spatial period of the calculated fluctuation is much longer than the observed spatial period. This suggests that other factors are contributing to the large experimental fluctuations.

IV. SURFACE SCATTERER NEAR A METAL SURFACE

In this section, we consider an impurity in the vicinity of a metal surface. The metal surface is modelled by a finite barrier $U_s(z)$ which is given by

$$U_s(z)=\begin{cases} U_0, & z>0 \\ 0, & z\le 0 \end{cases}, \tag{32}$$

where for later convenience we define U_0 in the form $U_0 \equiv \hbar^2 q^2/2m^*$. The impurity potential is assumed to be spherically symmetric and confined within a small muffin-tin radius. Although a screened potential close to a metal surface may be far from the spherically sym-

metric muffin-tin type, we expect the results from this simple model would still contain essential features of the real problem. We describe the scattering behavior in terms of the impurity scattering phase shifts. From now on, we assume that the impurity scatters electrons isotropically and keep only the s-wave phase shift δ_0.

For a plane-wave state $\mathbf{k}$ incident upon and reflected by the barrier alone, the resulting scattering state is given by

$$\phi_{\mathbf{k}^+}(\mathbf{r})=\frac{1}{\sqrt{\Omega}}\times\begin{cases}\dfrac{2k_z}{k_z+i(q^2-k_z^2)^{1/2}}e^{-(q^2-k_z^2)^{1/2}z}e^{i\mathbf{k}_\parallel\cdot\mathbf{r}_\parallel}, & z>0\\ e^{i\mathbf{k}^+\cdot r}+\dfrac{k_z-i(q^2-k_z^2)^{1/2}}{k_z+i(q^2-k_z^2)^{1/2}}e^{i\mathbf{k}^-\cdot\mathbf{r}}, & z\le 0\end{cases} \tag{33}$$

where $\mathbf{k}^{\pm}=\mathbf{k}_\parallel\pm k_z\hat{z}$, k_z is taken to be positive, and Ω is the volume of the system. Here $\mathbf{k}_\parallel=(k_x,k_y)$ and $\mathbf{r}_\parallel=(x,y)$. Now, in addition, we have an impurity with its position $\mathbf{r}_{\rm imp}=-b\hat{z}$. The total wave function outside the metal surface (i.e., $z>0$) is found (see the Appendix) to be

$$\phi^{(+)}_{\mathbf{k}^+}(\mathbf{r})=\frac{1}{\sqrt{\Omega}}\left[\frac{2k_z}{k_z+i(q^2-k_z^2)^{1/2}}e^{-(q^2-k_z^2)^{1/2}z}e^{i\mathbf{k}_\parallel\cdot\mathbf{r}_\parallel}+\frac{2i\sin\delta_0 e^{i\delta_0}}{\sqrt{4\pi}}A_0(k_z)B(\mathbf{r})\right] \tag{34}$$

where

$$\frac{A_0(k_z)}{\sqrt{4\pi}}=\frac{e^{-ik_zb}+\{[k_z-i(q^2-k_z^2)^{1/2}]/[k_z+i(q^2-k_z^2)^{1/2}]\}e^{ik_zb}}{1+i\sin\delta_0 e^{i\delta_0}C_0}, \tag{35}$$

and

$$B(\mathbf{r})=\frac{1}{k_{FB}}\int_0^\infty dK_\parallel\frac{K_\parallel J_0(K_\parallel r_\parallel)}{(k_{FB}^2-K_\parallel^2)^{1/2}+i(q^2+K_\parallel^2-k_{FB}^2)^{1/2}}e^{i(k_{FB}^2-K_\parallel^2)^{1/2}b}e^{-(q^2+K_\parallel^2-k_{FB}^2)^{1/2}z}. \tag{36}$$

In Eq. (35), the factor C_0 in the denominator is

$$C_0=-\frac{1}{q^2k_{FB}}\int_0^\infty dK_\parallel\frac{K_\parallel}{(k_{FB}^2-K_\parallel^2)^{1/2}}[(k_{FB}^2-K_\parallel^2)^{1/2}-i(q^2+K_\parallel^2-k_{FB}^2)^{1/2}]^2e^{2i(k_{FB}^2-K_\parallel^2)^{1/2}b}. \tag{37}$$

In Eq. (36), $J_0(K_\parallel r_\parallel)$ is the cylindrical Bessel function of order zero and $r_\parallel=(x^2+y^2)^{1/2}$. $B(\mathbf{r})$ is a function of $r_\parallel$ and z and is therefore cylindrically symmetrical. As in the previous section, the convention $(-1)^{1/2}=+i$ is implied in the integrands of both Eqs. (36) and (37).

For the metallic system, we assume uniform background scatterers which set up the transport-electron distribution as well as the transport field. In the following analysis, we consider the case where the transport electrons move along direction $\hat{x}$. The incident-electron distribution is described by $\mu_{\mathbf{k}}$, which is given by

$$\mu_{\mathbf{k}}=\begin{cases}\mu-eE_0l\hat{k}\cdot\hat{x}, & k_z>0\\ \mu, & k_z<0,\end{cases} \tag{38}$$

where $-E_0\hat{x}$ is the field set up by the background scatterers ($E_0>0$). The LTF is obtained from the general expression in Eq. (4) and from the wave function and electron distribution in Eqs. (34) and (38), respectively. The result in the region very close to the barrier ($z=0^-$) is given by

$$\delta V_{\rm LTF}(\mathbf{r}_\parallel)=\delta V_{\rm LTF}(r_\parallel)E_0l\cos\phi, \tag{39}$$

where

$$\delta V_{\rm LTF}(r_\parallel)=-\frac{2}{\sqrt{\pi}}\left[\frac{k_{FB}}{q}\right]^2\int_0^1 dx\; x(1-x^2)^{1/2}J_1[k_{FB}r_\parallel(1-x^2)^{1/2}]$$
$$\times{\rm Re}\{\sin\delta_0 e^{i\delta_0}A_0(k_{FB}x)B(\mathbf{r}_\parallel)[x+i(q^2-k_{FB}^2x^2)^{1/2}/k_{FB}]\}. \tag{40}$$

Here J_1 is the cylindrical Bessel function of order 1 and ϕ is the azimuthal angle. Similarly, the STM potential is obtained by substituting Eqs. (34) and (38) into the general expression (14). The result is

$$\delta V_{\rm STM}(\mathbf{r}_0)=\delta V_{\rm STM}(r_\parallel,z_0)(E_0l)\cos\phi, \tag{41}$$

where $\mathbf{r}_0=\mathbf{r}_\parallel+z_0\hat{z}$ is the position of the STM tip and

$$\delta V_{\mathrm{STM}}(r_{\parallel},z_0)=\frac{-\int_0^1 dx\, x(1-x^2)^{1/2}J_1[k_{FB}r_{\parallel}(1-x^2)^{1/2}]\exp[-(q^2-k_{FB}^2x^2)^{1/2}z_0]\mathrm{Re}F(x,\mathbf{r}_0)}{\int_0^1 dx\left[\left[\frac{2k_{FB}x}{q}\right]^2\exp[-2(q^2-k_{FB}^2x^2)^{1/2}z_0]+\frac{\sin^2\delta_0}{\pi}|A_0(k_{FB}x)B(\mathbf{r}_0)|^2-D(x,\mathbf{r}_0)\right]}, \tag{42}$$

where

$$F(x,\mathbf{r}_0)=\frac{4}{\sqrt{\pi}}\left[\frac{A_0(k_{FB}x)B(\mathbf{r}_0)\sin\delta_0 e^{i\delta_0}}{k_{FB}x-i(q^2-k_{FB}^2x^2)^{1/2}}\right]$$

and

$$D(x,\mathbf{r}_0)=k_{FB}xJ_0[k_{FB}r_{\parallel}(1-x^2)^{1/2}]e^{-(q^2-k_{FB}^2x^2)^{1/2}}e^{-(q^2-k_{FB}^2x^2)^{1/2}z_0}\mathrm{Im}F(x,\mathbf{r}_0)\ .$$

For numerical examples, we still take the metallic system to be aluminum ($k_{FB}=0.927$ a.u. and $U_0=1.36E_{FB}$). In Fig. 4 we present plots of the dimensionless potentials $\delta V_{\mathrm{LTF}}(r_{\parallel})$ and $\delta V_{\mathrm{STM}}(r_{\parallel},z_0)$ versus $r_{\parallel}$ measured in a.u. for the case $b=0$ a.u. This corresponds to a scatterer just inside the surface. The phase shift δ_0 is chosen to be 60°. (Similar behavior occurs for other values of δ_0.) According to their introduction in Eqs. (39) and (41), the dimensionless potentials which are plotted represent the actual potentials in units of $E_0 l$ which would be measured along a line starting just above the impurity and running along the direction of electron-particle current ($\phi=0$). $\delta V_{\mathrm{STM}}(r_{\parallel},z_0)$ is plotted for $z_0=2$, 4, and 6 a.u. The $\delta V_{\mathrm{LTF}}(r_{\parallel})$ curve is indicated by the dashed curve. From the figures, we see that a smaller z_0 gives rise to larger fluctuations. A large negative dip appears in the region very close to the scatterer. The position of the dip is about 2.2 a.u. from the scatterer. For the asymptotic region, when $r_{\parallel}$ is large, the LTF shows long-range oscillations. Numerical analysis reveals that

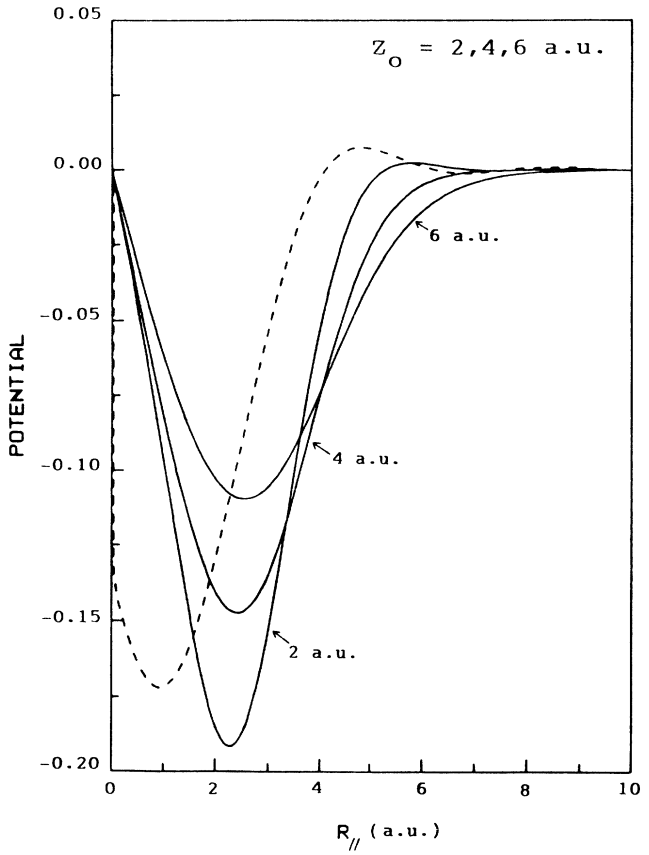

FIG. 4. Plots of $\delta V_{\mathrm{LTF}}(r_{\parallel})$ and $\delta V_{\mathrm{STM}}(r_{\parallel},z_0)$ vs $r_{\parallel}$ for the case of an impurity on an aluminum surface ($b=0$ a.u.). The values for the STM tip height z_0 are 2, 4, and 6 a.u. The impurity phase shift is $\delta_0=60°$. The δV_{LTF} curve is indicated by the dashed curve. The STM curves represent the measured STM potentials in units of $E_0 l$ as the STM tip is moved parallel to the surface from a position just above the impurity ($r_{\parallel}=0$) along a line in the direction of electron-particle current.

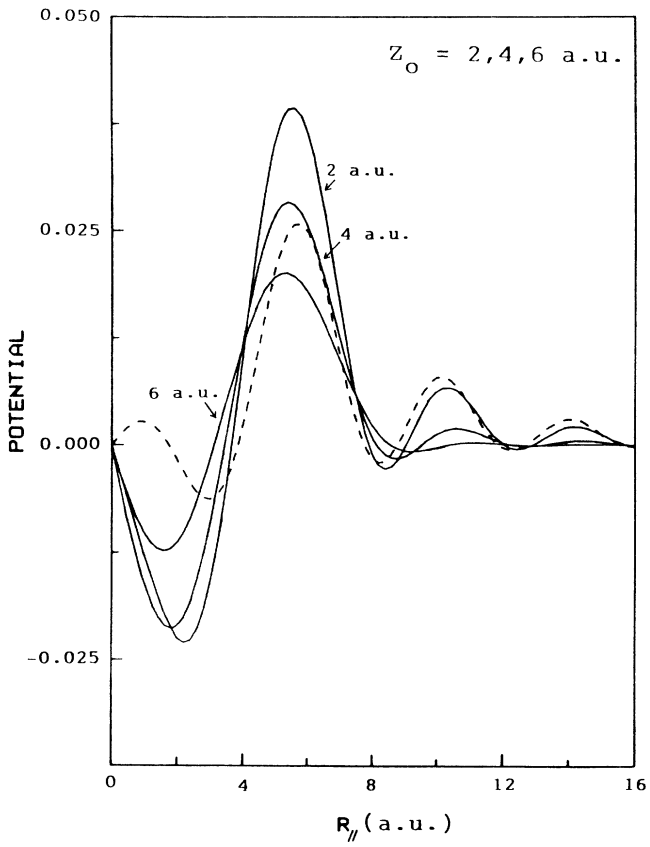

FIG. 5. Plots of $\delta V_{\mathrm{LTF}}(r_{\parallel})$ and $\delta V_{\mathrm{STM}}(r_{\parallel},z_0)$ vs $r_{\parallel}$ for the case of an impurity at position 5 a.u. inside an aluminum surface ($b=5$ a.u.) All other parameters are the same as in Fig. 4.

the amplitude of the long-range oscillations goes like $r_{\parallel}^{-4}$ in the asymptotic region. We also find that for $z_0=2$ and 4 a.u., $\delta V_{\rm STM}(r_{\parallel},z_0)$ and $\delta V_{\rm LTF}(r_{\parallel})$ vary in a similar way in the asymptotic region, and they are of the same order of magnitude. For $z_0=6$ a.u., $\delta V_{\rm STM}(r_{\parallel},z_0)$ is much smaller than $\delta V_{\rm LTF}(r_{\parallel})$ in the asymptotic region.

In Fig. 5, we present plots of $\delta V_{\rm LTF}(r_{\parallel})$ and $\delta V_{\rm STM}(r_{\parallel},z_0)$ versus $r_{\parallel}$ for the case $b=5$ a.u. The phase shift δ_0 is again chosen to be 60°. The negative dip in the close-in region is an order of magnitude smaller than that in Fig. 4, while the longer-range oscillations are of the same order of magnitude as those in Fig. 4. Again, as in Fig. 4, for the case $z_0=2$ and 4 a.u., $\delta V_{\rm STM}(r_{\parallel},z_0)$ and $\delta V_{\rm LTF}(r_{\parallel})$ vary in a similar way in the asymptotic region, and they are of the same order of magnitude. For $z_0=6$ a.u., $\delta V_{\rm STM}(r_{\parallel},z_0)$ is much smaller than $\delta V_{\rm LTF}(r_{\parallel})$ in the asymptotic region.

In general, from Eqs. (39) and (41), the azimuthal dependence of $\delta V_{\rm STM}$ and $\delta V_{\rm LTF}$ is the same as that of a dipole field. The $\delta V_{\rm LTF}$ and the $\delta V_{\rm STM}$ are of the same order of magnitude in the region close to the scatterer. However, except when the distance z_0 between the STM tip and the metal surface is very small ($z_0 \lesssim 2$ Å in our numerical examples), the $\delta V_{\rm STM}$ fails to trace the asymptotic spatial variation of the $\delta V_{\rm LTF}$. The asymptotic $\delta V_{\rm LTF}(\mathbf{r}_{\parallel})$ of a surface scatterer decreases like $r_{\parallel}^{-4}$ times a spatially oscillating factor, which is a consequence of interference between the incident electron wave and the scattered wave. Similar $r_{\parallel}^{-4}$ dependence is found in an infinite-barrier model when the impurity is just inside the surface.[17] For $r_{\parallel} \gg l$, the interference effect should be small and $\delta V_{\rm LTF}(\mathbf{r}_{\parallel})$ should vary as a dipole field in the radial direction. This would correspond to the asymptotic field of a residual resistivity dipole located near a metal surface.[2] This asymptotic field is not contained in our analysis because we have restricted attention to the near-field quantum-mechanical regime where $r_{\parallel} \gg l$.

We estimate that sub-μV sensitivity is needed in order that the $\delta V_{\rm STM}$ can effectively probe the close in $\delta V_{\rm LTF}$. Using the relation $E_0 l = 3\pi^2 \hbar J_0/(e^2 k_F^2)$, and assuming that the current density $J_0 \lesssim 10^6$ Amp/cm^2, we obtain $E_0 l \lesssim 4$ μV. From Fig. 4, for the case of a surface scatterer and for $z_0 \lesssim 3$ Å, a conservative estimate of the close-in variations of $\delta V_{\rm LTF}$ and $\delta V_{\rm STM}$ gives values on the order of 0.1 $(E_0 l) \lesssim 0.4$ μV. A scanning tunneling microscopy of sub-μV sensitivity is shown to be experimentally possible by Pelz *et al.*[5] Hence, for a close enough STM tip ($z_0 \lesssim 3$ Å), the change in $\delta V_{\rm STM}$ due to the presence of a surface scatterer in a transport situation should be experimentally observable.

V. DISCUSSION

A general theoretical approach is presented to analyze the local transport field and the STM potential in a current-carrying mesoscopic system. We have shown that the phase sensitivity of the STM voltage measurement gives rise to spatial variation of the STM voltage. The STM tip is a weak-coupling probe which does not couple equally to all subbands, but is more sensitive to the higher-occupied subbands. Hence $\delta V_{\rm STM}$ and $\delta V_{\rm LTF}$ do not have the same spatial variation. However, we have seen that the STM can still be used as a qualitative probe of the spatial profile of the local transport field. The phase-sensitivity of the STM measurements is not so pronounced as was found by Büttiker for 1D systems.[11] The point is that summing the distribution from different channels leads to the integrals and summations in Eqs. (28a), (28b), and (42). These integrals and summations introduce some phase averaging to $\delta V_{\rm STM}$ which results in decreasing interference as the distance from the scatterer is increased. We then expect the phase sensitivity to remain significant at all locations only in one-dimensional systems.[11,12] A possible realization of such a system is the narrow constriction having no more than a few propagating channels.

We have considered two situations: a thin-metal film containing grain boundaries and a scatterer on a metal surface. For a thin-metal film containing grain boundaries, the $\delta V_{\rm STM}$ is shown to fluctuate on a larger length scale than the local transport field. The phase sensitive $\delta V_{\rm STM}$ always oscillates about the phase-insensitive $\delta V_{\rm STM}$ value which is constant in space except for a step-like change across a grain boundary. We have considered three different incident-electron distributions for comparison. The $\delta V_{\rm STM}$ and the local transport field are of the same order of magnitude for all three incident-electron distributions. However, the incident-electron distributions that correspond to both the parallel semiclassical barriers and the background-τ cases have fewer electrons in the higher-occupied subbands. Hence the $\delta V_{\rm STM}$ and the local transport field have about the same spatial average. We have also shown that the fluctuation amplitude of $\delta V_{\rm STM}$ for typical parameter values is of the order of 1 μV, which should be observable experimentally.

For a scatterer on a metal surface, the $\delta V_{\rm STM}$ and the local transport field in the metal are of the same order of magnitude provided that the STM tip is not too far from the surface. In addition, the $\delta V_{\rm STM}$ has the azimuthal dependence which is typical of a dipole field. The radial dependence of the local transport field is not the same as in a dipole field in the regions where interference is important. However, in the region where $r \gg l$, where r is the distance from the scatterer, the local transport field is expected to become a dipole field.[2] Also, it appears that sub-μV sensitivity is needed for the STM to probe the effects of the local transport field in the vicinity of a surface scatterer.

In our analysis, we have idealized the STM probe to be able to probe a point on the surface at a time. For a more realistic consideration, we have to consider the finite size of the STM tip. The finite-sized tip should probe over a region on the surface and a first approximation would be to average our results over a small window corresponding to the lateral resolution of the STM. Our results are essentially unchanged for a window size less than 2 Å. Finally, we point out that we have not included incoherent scattering or inelastic-scattering explicitly, but we have implicitly assumed that incoherent scattering is involved in defining the incident-electron distribution. Therefore, our results are valid when the STM tip is much closer than a mean free path from the scatterer.

On the other hand, when the STM tip is on the order of a mean free path from the scatterer, incoherent scattering must be included in the quantum-mechanical scattering process. Further work is required to describe scanning tunneling potentiometry in this transition region.

ACKNOWLEDGMENTS

This work was supported by the Rome Air Development Center, United States Air Force.

APPENDIX

In this Appendix, we briefly outline the derivation that leads to Eq. (34). The derivation is simpler when the impurity is an s scatterer. However, it is straightforward to generalize beyond s scatterers and to include all phase shifts δ_l. It is convenient to express the wave functions in terms of spherical harmonics about the position of the impurity. The expansion of $\phi_{\mathbf{k}^+}(\mathbf{r})$, given by Eq. (33), is

$$\phi_{\mathbf{k}^+}(\mathbf{r})=\frac{1}{\sqrt{\Omega}}\sum_{l,m}A_{lm}^{(0)}j_l(k_{FB}|\mathbf{r}-\mathbf{r}_{\rm imp}|)Y_{lm}((\mathbf{r}-\mathbf{r}_{\rm imp})/|\mathbf{r}-\mathbf{r}_{\rm imp}|)\ , \tag{A1}$$

where

$$A_{lm}^{(0)}=4\pi i^l\left[e^{-ik_z b}Y_{lm}^*(\hat{k}^+)+\frac{k_z-i(q^2-k_z^2)^{1/2}}{k_z+i(q^2-k_z^2)^{1/2}}e^{ik_z b}Y_{lm}^*(\hat{k}^-)\right]\ . \tag{A2}$$

Here we have taken the energy to be the Fermi energy. If the scattering problem is exactly solved, the $A_{lm}^{(0)}$ will be renormalized to A_{lm} and substituting A_{lm} in place of $A_{lm}^{(0)}$ in (A1) gives the self-consistent wave incident upon the impurity. The total wave which scatters from the s-like impurity, is then given by $i\sin\delta_0 e^{i\delta_0}(A_{00}/\sqrt{4\pi\Omega})h_0^{(1)}(k_{FB}|\mathbf{r}-\mathbf{r}_{\rm imp}|)$. From now on, we define

$$A_{00}\equiv A_0\ . \tag{A3}$$

We now consider a spherical wave $h_0^{(1)}(k_{FB}|\mathbf{r}-\mathbf{r}_{\rm imp}|)$ incident upon the finite barrier. The spherical wave can be written in an integral form

$$h_0^{(1)}(k_{FB}|\mathbf{r}+b\hat{z}|)=\int d\mathbf{K}_\parallel e^{i\mathbf{K}_\parallel\cdot\mathbf{r}_\parallel}\frac{e^{i(k_{FB}^2-K_\parallel^2)^{1/2}|z+b|}}{2\pi k_{FB}(k_{FB}^2-K_\parallel^2)^{1/2}}\ , \tag{A4}$$

where $\mathbf{K}_\parallel\equiv(K_x,K_y)$. We allow each plane-wave component in the integrand of Eq. (A4) to be reflected from the surface barrier. The wave reflected from the finite barrier is

$$\frac{1}{q^2}\int d\mathbf{K}_\parallel e^{i\mathbf{K}_\parallel\cdot\mathbf{r}_\parallel}[(k_{FB}^2-K_\parallel^2)^{1/2}-i(q^2+K_\parallel^2-k_{FB}^2)^{1/2}]^2\frac{e^{i(k_{FB}^2-K_\parallel^2)^{1/2}b}}{2\pi k_{FB}(k_{FB}^2-K_\parallel^2)^{1/2}}e^{i(k_{FB}^2-K_\parallel^2)^{1/2}z}$$

and the s component of the reflected wave is defined by $-C_0\sqrt{4\pi}$ such that

$$-C_0\sqrt{4\pi}\equiv\frac{\sqrt{4\pi}}{q^2k_{FB}}\int_0^\infty dK_\parallel K_\parallel[(k_{FB}^2-K_\parallel^2)^{1/2}-i(q^2+K_\parallel^2-k_{FB}^2)^{1/2}]^2\frac{e^{2i(k_{FB}^2-K_\parallel^2)^{1/2}b}}{(k_{FB}^2-K_\parallel^2)^{1/2}}\ . \tag{A5}$$

The self-consistent condition is then given by

$$A_0=A_{00}^{(0)}-i\sin\delta_0 e^{i\delta_0}A_0C_0\ , \tag{A6}$$

or

$$A_0=\frac{A_{00}^{(0)}}{1+i\sin\delta_0 e^{i\delta_0}C_0}\ . \tag{A7}$$

The explicit expression for A_0 is given in Eq. (35). The final step is to find that part of the wave inside the vacuum region that is due to the scattered wave from the impurity. The total wave scattered from the impurity and incident upon the surface barrier is

$$\psi_{\rm imp}=\frac{i\sin\delta_0 e^{i\delta_0}A_0}{\sqrt{4\pi\Omega}}\int d\mathbf{K}_\parallel e^{i\mathbf{K}_\parallel\cdot\mathbf{r}_\parallel}\frac{e^{i(k_{FB}^2+K_\parallel^2)^{1/2}|z+b|}}{2\pi k_{FB}(k_{FB}^2-K_\parallel^2)^{1/2}}\ . \tag{A8}$$

Within the vacuum region, the wave due to the incident $\psi_{\rm imp}$ wave is given by

$$\psi_{\rm imp}^{\rm vacuum}=\frac{i\sin\delta_0 e^{i\delta_0}A_0}{\sqrt{4\pi\Omega}}\int d\mathbf{K}_\parallel \frac{e^{i\mathbf{K}_\parallel\cdot\mathbf{r}_\parallel}}{2\pi k_{FB}}\frac{e^{i(k_{FB}^2-K_\parallel^2)^{1/2}b}}{(k_{FB}^2-K_\parallel^2)^{1/2}}\frac{2(k_{FB}^2-K_\parallel^2)^{1/2}e^{-(q^2+K_\parallel^2-k_{FB}^2)^{1/2}z}}{(k_{FB}^2-K_\parallel^2)^{1/2}+i(q^2+K_\parallel^2-k_{FB}^2)^{1/2}} . \tag{A9}$$

We perform the angular integral of $\psi_{\rm imp}^{\rm vacuum}$ in Eq. (A9) and get

$$\psi_{\rm imp}^{\rm vacuum}=\frac{2i\sin\delta_0 e^{i\delta_0}A_0}{\sqrt{4\pi\Omega k_{FB}}}\int_0^\infty d\mathbf{K}_\parallel \frac{K_\parallel J_0(K_\parallel r_\parallel)}{(k_{FB}^2-K_\parallel^2)^{1/2}+i(q^2+K_\parallel^2-k_{FB}^2)^{1/2}}e^{i(k_{FB}^2-K_\parallel^2)^{1/2}b}e^{-(q^2+K_\parallel^2-k_{FB}^2)^{1/2}z} . \tag{A10}$$

Adding $\psi_{\rm imp}^{\rm vacuum}$ to the incident wave in the vacuum region gives Eq. (34).

---

[1]R. Landauer, IBM J. Res. Develop. **1**, 223 (1957); Z. Phys. B **21**, 247 (1975).

[2]R. S. Sorbello and C. S. Chu, IBM J. Res. Develop. **32**, 58 (1988).

[3]P. Muralt and D. W. Pohl, Appl. Phys. Lett. **48**, 514 (1986).

[4]J. R. Kirtley, S. Washburn, and M. J. Brady, Phys. Rev. Lett. **60**, 1546 (1988). See also J. R. Kirtley, S. Washburn, and M. J. Brady, Bull. Am. Phys. Soc. **34**, 538 (1989).

[5]J. P. Pelz and R. H. Koch, Rev. Sci. Instrum. **60**, 301 (1989).

[6]R. Landauer, in *Electrical Transport and Optical Properties in Inhomogeneous Media,* edited by J. C. Garland and D. B. Tanner (AIP, New York, 1978), p. 2.

[7]C. S. Chu and R. S. Sorbello, Phys. Rev. B **40**, 5950 (1989).

[8]R. S. Sorbello, Phys. Rev. B **39**, 4984 (1989).

[9]C. S. Chu and R. S. Sorbello, Phys. Rev. B **38**, 7260 (1988).

[10]J. Tersoff and D. R. Hamann, Phys. Rev. Lett. **50**, 1998 (1983).

[11]M. Büttiker, Phys. Rev. B **40**, 3409 (1989).

[12]M. Büttiker, in *Analogies in Optics and Micro-Electronics,* edited by W. van Haeringen and D. Lenstra (Kluwer Academic, Dordrecht, 1990).

[13](a) M. Büttiker, IBM J. Res. Develop. **32**, 317 (1988); (b) For the case of reservoirs attached to the ends of the sample, Eq. (7) is equivalent to Eq. (51) of (a).

[14]M. Bütiker, Y. Imry, R. Landauer, and S. Pinhas, Phys. Rev. B **31**, 6207 (1985).

[15]A. Seeger, Can. J. Phys. **34**, 1219 (1956); J. R. Smith and J. Ferrante, Phys. Rev. B **34**, 2238 (1986).

[16]For our confining potential, given in Eq. (13), the weighting factor $|\phi_n(z_0)|^2$ is

$$|\phi_0(z_0)|^2=\begin{cases}e^{-2\beta d}\left[\dfrac{1}{\beta}+\dfrac{W(1+\xi^{-1}\sin\theta)}{2\cos^2(\xi/2)}\right]^{-1} & \text{for odd } n\\ e^{-2\beta d}\left[\dfrac{1}{\beta}+\dfrac{W(1-\xi^{-1}\sin\xi)}{2\sin^2(\xi/2)}\right]^{-1} & \text{for even } n\ ,\end{cases}$$

where $d=z_0-W/2$ is the distance of the STM tip from the film surface, $\beta=[2m^*(U_0-E_n)/\hbar^2]^{1/2}$, and $\xi=W(2m^*E_n/\hbar^2)^{1/2}$.

[17]C. S. Chu and R. S. Sorbello (unpublished).